PHYSICAL REVIEW LETTERS

Two-Dimensional Superconducting Phase in $LaTiO_3/SrTiO_3$ Heterostructures Induced by High-Mobility Carrier Doping

J. Biscaras,[1] N. Bergeal,[1] S. Hurand,[1] C. Grossetête,[1] A. Rastogi,[2] R. C. Budhani,[2,3] D. LeBoeuf,[4]
C. Proust,[4] and J. Lesueur[1]

[1]*LPEM-UMR8213/CNRS-ESPCI ParisTech-UPMC, 10 rue Vauquelin-75005 Paris, France*
[2]*Condensed Matter-Low Dimensional Systems Laboratory, Department of Physics, Indian Institute of Technology Kanpur,
Kanpur 208016, India*
[3]*National Physical Laboratory, New Delhi-110012, India*
[4]*Laboratoire National des Champs Magnétiques Intenses, UPR 3228, (CNRS-INSA-UJF-UPS), Toulouse 31400, France*
(Received 16 November 2011; published 15 June 2012)

In this Letter, we show that a superconducting two-dimensional electron gas is formed at the
$LaTiO_3/SrTiO_3$ interface whose transition temperature can be modulated by a back-gate voltage. The
gas consists of two types of carriers: a majority of low-mobility carriers always present, and a few high-
mobility ones that can be injected by electrostatic doping. The calculation of the electron spatial
distribution in the confinement potential shows that the high-mobility electrons responsible for super-
conductivity set at the edge of the gas whose extension can be tuned by the field effect.

Oxide-based heterostructures appear as serious chal-
lengers for future electronics as they offer a great variety
of electronic orders suitable to achieve new functionalities
[1,2]. A key issue for oxide electronics to emerge is the
ability to tune these properties with an electric field. The
discovery of a high-mobility two-dimensional electron gas
(2DEG) in oxide heterostructures is a milestone on this
road [3]. $SrTiO_3$-based structures attracted much attention
in this context, since (i) large mobility can be obtained;
(ii) their complex phase diagram includes various
electronic orders such as superconductivity [4–6] and mag-
netism [7–9]; and (iii) their carrier density can be electro-
statically modulated [10,11]. However, the electrostatic
control of the 2DEG properties is not fully understood
yet. Here we show that superconductivity at the
$LaTiO_3/SrTiO_3$ interface can be turned on and controlled
by injection of a few highly mobile electrons.

The $LaTiO_3/SrTiO_3$ perovskite heterostructure is par-
ticularly interesting in the context of $SrTiO_3$-based inter-
faces since it is made of TiO_2 planes as building blocks,
where the Ti atoms can have multiple valence values.
$SrTiO_3$ is a well known band insulator with a 3.2 eV
band gap with Ti atoms in the $3d^0$ (4^+) configuration. On
the other hand, $LaTiO_3$ is an antiferromagnetic Mott insu-
lator with Ti atoms in the $3d^1$ (3^+) configuration.
Therefore, when a thin layer of $LaTiO_3$ is epitaxially
grown on a TiO_2 terminated $SrTiO_3$ substrate, half an
electron per unit cell is available to form a 2DEG confined
at the interface, as confirmed by band structure calculations
[12]. We have shown recently that the electron gas extends
a few unit cells in the $SrTiO_3$ layer and undergoes a super-
conducting transition at low temperature (~ 200 mK) [5].
In this Letter, we investigate the phase diagram of
$LaTiO_3/SrTiO_3$ interfaces by electronic transport

measurements at low temperature (20 mK) and high field
(45 T) as a function of a back-gate voltage. $LaTiO_3$ epi-
taxial layers were grown on (100) $SrTiO_3$ single crystals
using pulsed laser deposition as described in Ref. [5].
Samples are cut in rectangular shapes along the two or-
thogonal in plane directions, hereafter referred as XX and
YY. A metallic titanium layer was deposited at the rear of
the 0.5 mm thick $SrTiO_3$ substrate to form an electrostatic
back gate. After the sample is cooled down, the gate
voltage V_G is ramped up to +200 V. This procedure
insures that all voltage sweeps made subsequently are
reversible and reproducible.

Figures 1(a) and 1(b) display the sheet resistance R_S of a
15 unit cell thick sample (sample A) as a function of
temperature for different values of the gate voltage V_G.
The normal state resistance, its temperature dependence,
and the superconducting critical temperature T_c strongly
depend on V_G. A superconducting to insulator transition
takes place as carriers are removed from the 2DEG. T_c has
a maximum of ~ 200 mK when adding electrons, and is
suppressed when the gate voltage becomes negative. This
suppression is correlated to a singular behaviour of the
normal resistance near $V_G = 0$ [Fig. 1(c)], indicating that
the gate voltage not only controls the carrier density, but
also modifies deeply the electronic properties of the 2DEG.

The Hall resistance R_{Hall} was measured at low magnetic
field ($B < 5$ T) as a function of gate voltage. The apparent
Hall electron density $n_{Hall} = B/eR_{Hall}$, which ranges from
3 to 5×10^{13} cm^{-2}, starts rising from $V_G = -200$ V as
expected for negative carriers, but drops surprisingly for
positive gate voltage [Fig. 2(b)]. The mobility $\mu_{Hall} =
1/en_{Hall}R_S$ is constant for $V_G < 0$, and then rises abruptly
for $V_G > 0$ [Fig. 2(c), purple squares]. Measurements per-
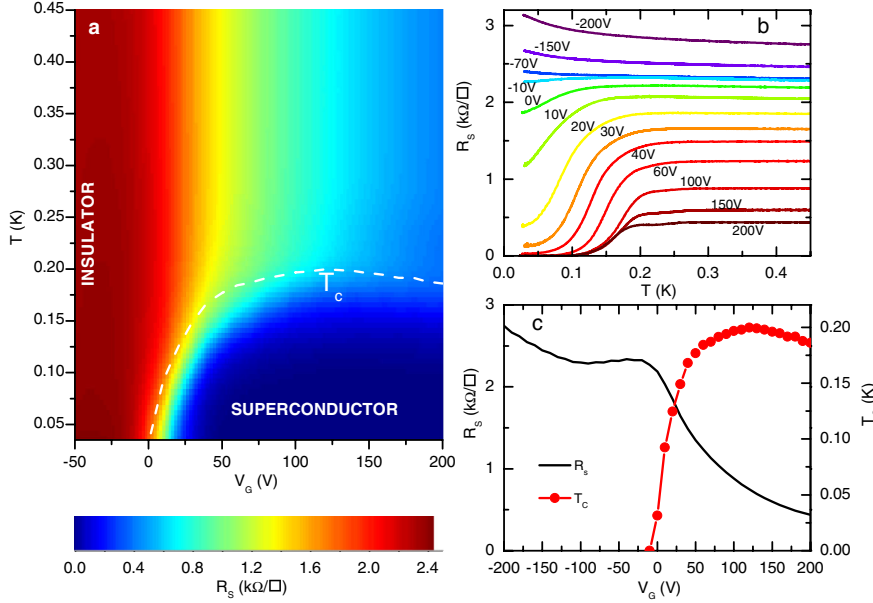formed at a higher magnetic field (45 T) reveal that the Hall

FIG. 1 (color online). Superconducting transition as a function of gate voltage for sample *A* (*XX* direction). (a) Sheet resistance of sample A in color scale as a function of temperature and gate voltage from -50 V to $+200$ V; the superconducting transition temperature (defined as a 15% drop in sheet resistance) is superimposed as a white dashed line (see Part I of the Supplemental Material [19] for a discussion on the T_c criterion). (b) Sheet resistance as a function of temperature for selected gate voltages. (c) Sheet resistance at 450 mK (left scale) and superconducting transition temperature (right scale) as a function of gate voltage (see Part II of the Supplemental Material [19] for the *YY* direction).

resistance is linear only for negative V_G, and not for positive V_G [Fig. 2(a)]. In the latter case, two distinct slopes are evidenced at low and high fields, respectively, suggesting a multiband transport scenario. In Fig. 2(a), the Hall resistance at high magnetic field has been fitted with a two-band model:

$$R_{\text{Hall}} = \frac{B}{e} \frac{\frac{n_1\mu_1^2}{1+\mu_1^2 B^2} + \frac{n_2\mu_2^2}{1+\mu_2^2 B^2}}{\left[\frac{n_1\mu_1}{1+\mu_1^2 B^2} + \frac{n_2\mu_2}{1+\mu_2^2 B^2}\right]^2 + \left[\frac{n_1\mu_1^2 B}{1+\mu_1^2 B^2} + \frac{n_2\mu_2^2 B}{1+\mu_2^2 B^2}\right]^2}, \quad (1)$$

where n_1 and n_2 are the 2D electron densities, and μ_1 and μ_2 the corresponding mobilities, with the constraint $1/R_s = en_1\mu_1 + en_2\mu_2$. As reported in Figs. 2(b) and 2(c), low and constant mobility μ_1 carriers (hereafter referred as LMC) are present for all gate biases, whereas a few highly mobile electrons (hereafter referred to as HMC) with a mobility μ_2 increasing linearly with bias, show up for positive V_G only, as also observed by Kim *et al.* [13]. As expected for electrostatic doping, the total number of carriers $n_{\text{total}} = n_1 + n_2$ rises monotonically with V_G (from 3 to 7×10^{13} cm^{-2}).

Such gate voltage dependent behaviour has been measured in all our samples, as for example the one reported in Fig. 3 (sample B), whose total carrier density is slightly higher (from 6 to 10×10^{13} cm^{-2}). The dependence of n_{total} with V_G has been confirmed by measuring the capacitance $C(V_G)$ between the back gate and the 2DEG and integrating it over the voltage range to obtain the electrostatic sheet carrier density

$$n_S(V_G) = n_S(V_G = -200 \text{ V}) + \frac{1}{eA}\int_{-200}^{V_G} C(V)dV, \quad (2)$$

where A is the area of the capacitor. As shown in Fig. 3(a), n_S superimposes perfectly on n_{Hall} at negative voltage, as expected since there is only one type of carrier. At positive

voltage, it matches n_{total} extracted from the two-band model analysis of high-field measurements. The sigmoid shape of the total number of carriers at low temperature is characteristic of the dielectric constant ϵ_R of the SrTiO$_3$ substrate, which is highly nonlinear and strongly temperature dependent below ~ 50 K as SrTiO$_3$ undergoes a transition to a quantum paraelectric phase [14,15]. At higher temperatures, $C(V_G)$ is constant, the total number of carriers rises linearly with V_G and equals the Hall number of carriers in the entire voltage range ($n_{\text{total}} = n_{\text{Hall}}$), indicating that no HMC are present in the 2DEG. As seen in Fig. 3(b), the mobility is also constant at this temperature, with the same value as the one measured at low temperature and negative V_G. When lowering the temperature below 50 K, the low-field Hall mobility rises up by more than an order of magnitude at $V_G = 200$ V, and the low-field Hall carrier density departs from the integrated capacitance measurements for $V_G > 0$ only. This is a strong indication that the two-band scenario is intrinsically related to the nonlinear variation of the SrTiO$_3$ dielectric constant ϵ_R in the quantum paraelectric regime.

To model the 2DEG properties, we have solved the coupled Schrödinger and Poisson equations self consistently, taking into account the dependence of ϵ_R with V_G and the continuity of the potential in the whole sample. Indeed, the gate voltage not only controls the total number of carriers in the 2DEG, but also the profile of the conduction band in the substrate. As opposed to previous calculations [16–18], we do not use a wedge-shape potential to model the confining potential of the 2DEG at the interface, since it cannot provide a continuous solution with the bulk band bending. Details of the calculations are given in Part III of the Supplemental Material [19]. The self consistent potential profile, as depicted for different V_G in Figs. 4(a)–4(c) for sample A, is made of a deep
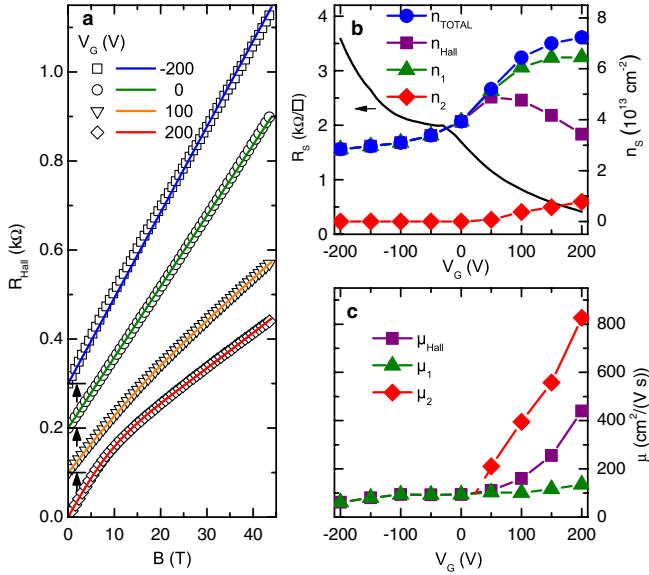
FIG. 2 (color online). Hall effect and two carrier analysis. (a) Hall resistance as a function of magnetic field for different gate voltages measured at 4.2 K on sample A (YY direction). Open symbols correspond to experimental data, and full lines to fits with Eq. (1). An offset, indicated by a black horizontal segment and an arrow, has been added to separate the curves. (b) Sheet resistance (left scale) and carrier density (right scale) extracted from Eq. (1) as a function of gate voltage measured at 4.2 K. n_1 (n_2) corresponds to LMC (HMC), n_{total} to the total density of carriers and n_{Hall} to the low-field Hall number. (c) Mobilities μ_1, μ_2, and μ_{Hall} corresponding to LMC, HMC, and the low-field Hall number extracted from Eq. (1).

potential well of typical width 2 nm, which accommodates a few subbands located in the vicinity of the interface (see Part V of the Supplemental Material [19] for sample B). For positive gate voltage, higher subbands filled up to the top of the conduction band profile extend up to 7 nm within the SrTiO$_3$ substrate. The corresponding carrier density profiles show a dominant contribution of carriers located at the interface, with a pronounced 2D character and therefore more subject to localization, which we assign to the LMC observed experimentally, and a minor contribution of more delocalized carriers at positive V_G, corresponding to the HMC. The extension of the gas reported in Fig. 4(d) is consistent with experimental results obtained on SrTiO$_3$-based interfaces [4,5,17,20]. It increases significantly for $V_G > 0$, as does the measured HMC density.

The origin of this peculiar behavior is deeply related to variations in the SrTiO$_3$ dielectric constant ϵ_R, which is highly electric field dependent at low temperature, and therefore changes locally within the heterostructure. As reported in Figs. 4(a)–4(c), the potential well is deep at the interface, and the corresponding electric field so high that ϵ_R decreases to its lower value whatever the gate voltage is, leading to a strong confinement of the gas. For $V_G < 0$, the band bending reinforces this feature. For
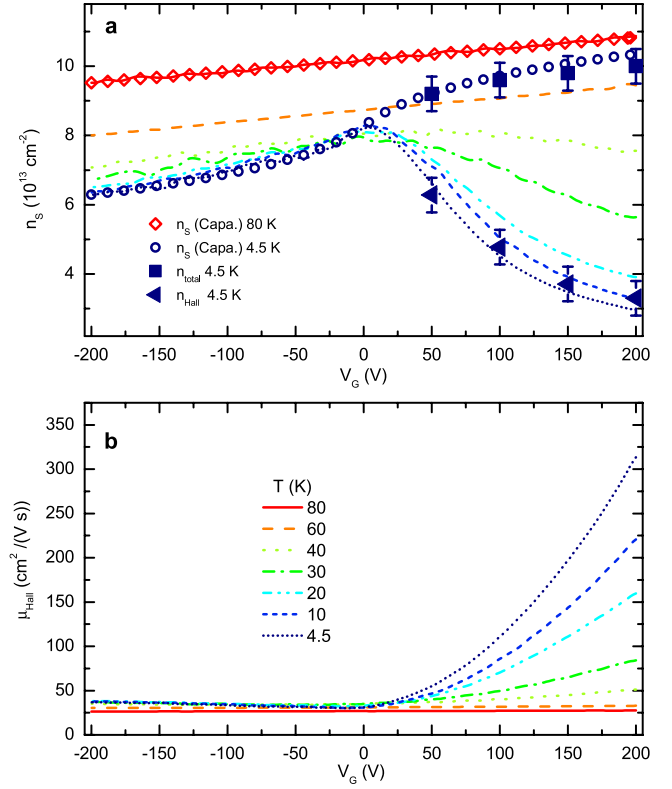

FIG. 3 (color online). Evolution of carrier density and mobility as a function of gate voltage and temperature. (a) Low-field (5 T) Hall number of carriers (full lines) and total number of carriers extracted from capacitance measurements (open symbols) as a function of gate voltage measured at different temperatures on sample B. Total number (squares) and low-field Hall number (triangles) extracted from the two carrier analysis of high-field experiments (45 T) are superimposed to the other curves, showing a very good agreement. (b) Hall mobility corresponding to low-field measurements as a function of gate voltage at the same temperatures. Beyond 60 K, that is, when the nonlinearity of ϵ_R strongly decreases, n_S and μ_{Hall} recover regular behavior with the gate voltage, that is, a rather constant mobility and a linear increase of the carriers concentration expected for a single carrier fluid.

$V_G > 0$, the edge of the well becomes shallower, the local electric field smaller, and ϵ_R starts rising towards the bulk, enhancing the deconfinement of the carriers. Their mobility gradually increases as the positive voltage is raised because the 2DEG extends away from the interface where the scattering is stronger [21] and anisotropic [22] (see Part II of the Supplemental Material [19]). This mechanism does not apply at high temperature when ϵ_R becomes field independent, and the LMC are solely observed above 60 K, as reported here (see Fig. 3). According to our model, the gate voltage not only controls the carrier density, but also the 2DEG spatial extension and its transport properties. The vicinity of $V_G = 0$ appears to be a turning point beyond which, for positive bias, mobile carriers are injected away from the interface. As can be seen in Fig. 4(d),
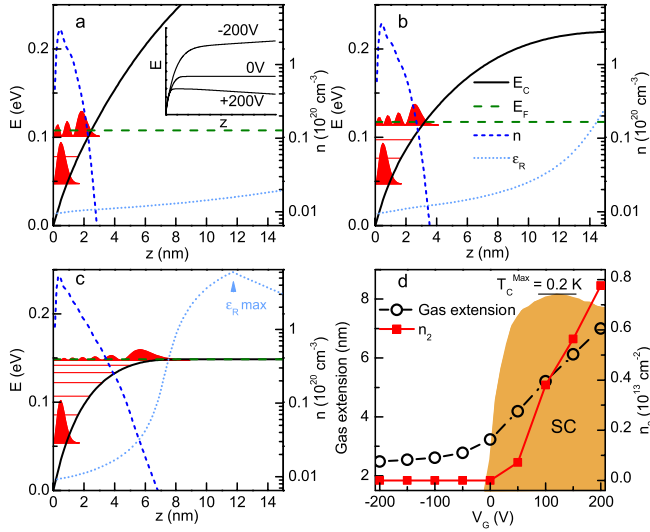
FIG. 4 (color online). Subband filling calculation in the interface potential well. (a–c) SrTiO$_3$ band bending calculation for three different gate voltages (-200 V, 0 V, $+200$ V) obtained with the experimental sheet carrier densities of Fig. 2(c). The figure displays the conduction band profile E_C (black), the Fermi energy E_F (green dashed), the subband energies (red), and the carrier density n (deep blue, left scale) as a function of depth z from the interface. The dielectric constant ϵ_R as a function of z is drawn on a log scale from 260 to 26000 (see Fig. 4 of the Supplemental Material [19] for the precise scale). The square modulus of the envelope function of the first and last filled subbands is indicated in arbitrary units (red areas). Inset: conduction band profile E_C at larger scale (0–100 nm) for the three different gate voltages. (d) 2DEG extension from the interface taken as the crossing point of E_C and E_F (left scale) and carrier density n_2 of HMC (right scale) as a function of gate voltage. The superconducting transition temperature as measured in Fig. 1(c) is superimposed with the same scale, as a reminder.

superconductivity is intimately related to the appearance of the HMC and their deconfinement within the SrTiO$_3$ substrate.

At first sight, the dome shape of T_c as a function of gate voltage observed at the LaTiO$_3$/SrTiO$_3$ interface may look like the bulk doped SrTiO$_3$ one [23]. However, the 3D carrier concentration at the interface [Figs. 4(a)–4(c)], even for the most negative gate bias, always reaches the range where bulk superconductivity is observed (i.e., from 10^{19} to 5×10^{20} cm^{-3}), whereas our samples are superconducting only when HMC are present. There is clearly something specific to the interface and to the carrier distribution profile. We can rule out a dimensionality driven transition, since the Fermi wavelength of the 2DEG is always larger than the gas expansion according to our model: the system remains 2D in the whole gate voltage range explored here. On the other hand, we see in Fig. 4(c) that as the gas extends within the substrate, i.e., at positive V_G, ϵ_R approaches the bulk SrTiO$_3$ value in the region where HMC set. Therefore, in this region, the situation could be similar to the one of bulk doped SrTiO$_3$, with a finite carrier

concentration in SrTiO$_3$ of high dielectric constant. The mechanism of superconductivity in SrTiO$_3$ is still under debate, but most of the theoretical models [24–26] take into account the polar properties of SrTiO$_3$ and its correlated peculiar dielectric constant to explain the superconducting properties and the dome-shaped phase diagram. Along these lines, superconductivity would appear at positive gate voltage in our LaTiO$_3$/SrTiO$_3$ heterostructures because the gas extends rather deep in the SrTiO$_3$ substrate, and T_c would decrease at high voltage as it does in bulk material. In that scenario, a full microscopic calculation of T_c with varying ϵ_R is needed, which is not available yet to compare with. Our data also point toward another key ingredient in the problem, the strong scattering at the interface. It is well known that disorder suppresses superconductivity through the enhancement of localization and electron-electron interactions (see, for instance, [27]). This may explain why for negative gate voltages, when only LMC are present at the interface, the 2DEG no longer displays superconductivity. On the other hand, superconductivity is rapidly restored as soon as HMC are injected. Even if this situation looks like a regular disorder-driven superconductor to insulator transition [28], the presence of two fluids spatially separated as depicted here is a unique situation, which has not yet been described theoretically.

Multiple carrier behavior has been reported in LaTiO$_3$/SrTiO$_3$ heterostructures [13,29]. The complex band structure of doped bulk SrTiO$_3$ [30] is a natural source of multicarrier transport properties. Moreover, electronic reconstruction calculations at LaTiO$_3$/SrTiO$_3$ interfaces clearly show that the band structure evolves within a few unit cells from the interface: the weight of Ti $3d_{xy}$ orbitals with a strong 2D character decays over 1 or 2 unit cells [12,31,32]. In this case, LMC and HMC would refer to carriers belonging to different subbands spatially distinct on a very short scale, less than a nanometer, which is 5 to 10 times shorter than our estimation for the HMC deconfinement. Other SrTiO$_3$-based heterostructures also display multicarrier transport properties [16,21,33] and deconfined HMC on the 5–10 nm scale [20], whereas calculations also point toward short scale (1 to 2 unit cells) electronic reconstruction [34]. Therefore, the occurrence of deconfined HMC, whose properties do not strongly depend on the details of the surface reconstruction, is a rather general feature of SrTiO$_3$-based heterostructures or even SrTiO$_3$ surfaces [35] and the two types of carriers are not simply related to bulk doped SrTiO$_3$ multibands. Moreover, when electrostatic doping is used, HMC appear at positive gate voltages in most systems [13,16], in line with the model we present in this article.

In summary, superconductivity in LaTiO$_3$/SrTiO$_3$ interfaces can be modulated with a back-gate voltage. In that case, we show that superconductivity is strongly correlated to the injection of highly mobile carriers at the edge of the 2DEG, whose extension increases rapidly with positive

gate voltage, because of the conduction band bending of $SrTiO_3$. This sheds new light on the phase diagram of the 2DEG at $LaTiO_3/SrTiO_3$ interface, and more generally on the other $SrTiO_3$-based interfaces, since the gate voltage appears not only as a way of tuning the carrier density, but also the geometry of the gas. Clearly, the 2DEG transport properties appear as a combination of those of carriers rather "deep" (a few nanometers) in bulk $SrTiO_3$, and those of carriers next to the interface, and therefore more sensitive to the details of the surface and/or electronic reconstructions [36]. That may explain why, if the overall picture among the different systems looks similar, striking differences can occur, such as the observation of magnetism by transport measurements in $LaAlO_3/SrTiO_3$ interfaces [7,9] in contrast to $LaTiO_3/SrTiO_3$ ones. The occurrence of different electronic orders (superconductivity, ferromagnetism, antiferromagnetism, etc.), their interactions and/or competitions, together with the transition to an insulating state may depend on the carrier density and on the gas extension tuned by the gate voltage. Our results open the way to a new description of the superconductor to insulator transition in these systems, and beyond, to a comprehensive understanding of the 2DEG physics at oxide interfaces.

[1] H. Takagi and H. Y. Hwang, Science **327,** 1601 (2010).

[2] J. Mannhart and D. G. Schlom, Science **327,** 1607 (2010).

[3] A. Ohtomo and H. Y. Hwang, Nature (London) **427,** 423 (2004).

[4] N. Reyren et al., Science **317,** 1196 (2007).

[5] J. Biscaras, N. Bergeal, A. Kushwaha, T. Wolf, A. Rastogi, R. C. Budhani, and J. Lesueur, Nature Commun. **1,** 89 (2010).

[6] Y. Kozuka, M. Kim, C. Bell, B. G. Kim, Y. Hikitam, and H. Y. Hwang, Nature (London) **462,** 487 (2009).

[7] A. Brinkman, M. Huijben, M. van Zalk, J. Huijben, U. Zeitler, J. C. Maan, W. G. van der Wiel, G. Rijnders, D. H. A. Blank, and H. Hilgenkamp, Nature Mater. **6,** 493 (2007).

[8] J. A. Bert, B. Kalisky, C. Bell, M. Kim, Y. Hikita, H. Y. Hwang, and K. A. Moler, Nature Phys. **7,** 767 (2011).

[9] L. Li, C. Richter, J. Mannhart, and R. C. Ashoori, Nature Phys. **7,** 762 (2011).

[10] S. Thiel, G. Hammerl, and A. Schmehl, Science **313,** 1942 (2006).

[11] A. Caviglia, S. Gariglio, N. Reyren, D. Jaccard, T. Schneider, M. Gabay, S. Thiel, G. Hammerl, J. Mannhart, and J.-M. Triscone, Nature (London) **456,** 624 (2008).

[12] P. Larson, Z. S. Popović, and S. Satpathy, Phys. Rev. B **77,** 245122 (2008).

[13] J. S. Kim, S. S. A. Seo, M. F. Chisholm, R. K. Kremer, H.-U. Habermeier, B. Keimer, and H. N. Lee, Phys. Rev. B **82,** 201407 (2010).

[14] R. Neville, C. Mead, and B. Hoeneise, J. Appl. Phys. **43,** 2124 (1972).

[15] J. Hemberger, P. Lunkenheimer, R. Viana, R. Bohmer, and A. Loidl, Phys. Rev. B **52,** 13 159 (1995).

[16] C. Bell, S. Harashima, Y. Kozuka, M. Kim, B. G. Kim, Y. Hikita, and H. Y. Hwang, Phys. Rev. Lett. **103,** 226802 (2009).

[17] O. Copie et al., Phys. Rev. Lett. **102,** 216804 (2009).

[18] K. Ueno, S. Nakamura, H. Shimotani, A. Ohtomo, N. Kimura, T. Nojima, H. Aoki, Y. Iwasa, and M. Kawasaki, Nature Mater. **7,** 855 (2008).

[19] See Supplemental Material at http://link.aps.org/supplemental/10.1103/PhysRevLett.108.247004 for more experimental results and more details on calculations.

[20] A. Dubroka et al., Phys. Rev. Lett. **104,** 156807 (2010).

[21] S. S. A. Seo, Z. Marton, W. S. Choi, G. W. J. Hassink, D. H. A. Blank, H. Y. Hwang, T. W. Noh, T. Egami, and H. N. Lee, Appl. Phys. Lett. **95,** 082107 (2009).

[22] At negative voltage, the anisotropy of the resistance is stronger (see Part II of the Supplemental Material [19]), showing that the scattering is more anisotropic. This is an indication that the 2DEG is close to the surface where surface reconstructions occurs.

[23] C. S. Koonce, M. L. Cohen, and J. Schooley, Phys. Rev. **163,** 380 (1967).

[24] J. Appel, Phys. Rev. Lett. **17,** 1045 (1966).

[25] Y. Takada, J. Phys. Soc. Jpn. **49,** 1267 (1980).

[26] C. S. Koonce and M. L. Cohen, Phys. Rev. **177,** 707 (1969).

[27] A. M. Finkel'stein, JETP Lett. **45,** 46 (1987).

[28] A. M. Goldman, Int. J. Mod. Phys. B **24,** 4081 (2010).

[29] R. Ohtsuka, M. Matvejeff, N. Nishio, R. Takahashi, and M. Lippmaa, Appl. Phys. Lett. **96,** 192111 (2010).

[30] L. F. Mattheis, Phys. Rev. B **6,** 4718 (1972).

[31] S. Okamoto and A. J. Millis, Nature (London) **428,** 630 (2004).

[32] Z. S. Popovic and S. Satpathy, Phys. Rev. Lett. **94,** 176805 (2005).

[33] Y. Hotta, T. Susaki, and H. Y. Hwang, Phys. Rev. Lett. **99,** 236805 (2007).

[34] Z. S. Popovic, S. Satpathy, and R. Martin, Phys. Rev. Lett. **101,** 256801 (2008).

[35] W. Meevasana, P. D. C. King, R. H. He, S-K. Mo, M. Hashimoto, A. Tamai, P. Songsiriritthigul, F. Baumberger, and Z-X. Shen, Nature Mater. **10,** 114 (2011).

[36] S. S. A. Seo, W. S. Choi, H. N. Lee, L. Yu, K. W. Kim, C. Bernhard, and T. W. Noh, Phys. Rev. Lett. **99,** 266801 (2007).